Sustainable Marine Structures
https://journals.nasspublishing.com/index.php/sms

ARTICLE

Eco-Efficient Vessel Dynamics: An Interval Approach to Heave Response and Energy-Saving in Rough Seas

Suleiman Mohammad [1,2], ***Markala Karthik*** [3], ***Yogeesh Nijalingappa*** [3,4*], ***Hanan Jadallah*** [1], ***Asokan Vasudevan*** [2,5], ***Azizbek Matmuratov*** [6], ***Mashkhura Sultonova*** [7]

[1] *Department of Electronic Marketing and Social Media, Economic and Administrative Sciences, Zarqa University, Zarqa 13132, Jordan*

[2] *Faculty of Business and Communications, INTI International University, Nilai 71800, Malaysia*

[3] *Department of Electrical and Electronics Engineering, SR University, Warangal 506371, India*

[4] *Department of Mathematics, Government First Grade College, Tumkur 572102, India*

[5] *School of Management, Shinawatra University, Samkhok 12160, Thailand*

[6] *Department of Pedagogical Sciences, Mamun University, Khiva 220900, Uzbekistan*

[7] *Department of Pedagogy and Psychology, Urgench State University Named after Abu Raykhan Beruniy, Urgench 220100, Uzbekistan*

ABSTRACT

Maritime transport faces increasing pressure to reduce fuel consumption and emissions, yet vessel performance under variable sea states remains difficult to bound reliably. Traditional stochastic and data-driven models provide probabilistic forecasts but lack strict guarantees in extreme or out-of-sample conditions. This study develops a deterministic arithmetic-interval framework that replaces uncertain hydrodynamic parameters and wave forcing with bounded intervals. The vessel's single-degree-of-freedom heave equation is reformulated as an interval differential equation, and existence and uniqueness of the resulting solution tube are established. Validated numerical techniques-interval Taylor expansions, Picard iteration, and adaptive subdivision-are used to compute tight

*CORRESPONDING AUTHOR:
Yogeesh Nijalingappa, Department of Electrical and Electronics Engineering, SR University, Warangal 506371, India; Department of Mathematics, Government First Grade College, Tumkur 572102, India; Email: yogeesh.r@gmail.com

ARTICLE INFO
Received: 10 September 2025 | Revised: 9 October 2025 | Accepted: 23 December 2025 | Published Online: 16 January 2026
DOI: https://doi.org/10.36956/sms.v8i1.2718

CITATION
Mohammad, S., Karthik, M., Nijalingappa, Y., et al., 2026. Eco-Efficient Vessel Dynamics: An Interval Approach to Heave Response and Energy-Saving in Rough Seas. Sustainable Marine Structures. 8(1): 41–63. DOI: https://doi.org/10.36956/sms.v8i1.2718

heave envelopes. An interval energy metric integrates worst-case power demand over a voyage, and a branch-and-bound global optimizer selects control parameters (e.g., speed schedules) that minimize the upper-bound energy while satisfying seakeeping constraints. Two hypothetical Karnataka-coast scenarios ("calm" and "rough" seas) demonstrate the rigor and efficiency of the approach. Computed energy-consumption intervals exactly enclose corresponding Monte-Carlo extremes, confirming tightness without large sample sizes. Rough-sea conditions increase worst-case energy demand by approximately 75% despite negligible heave amplitudes at the micron scale. Sensitivity analysis shows that wave-amplitude uncertainty dominates energy variability, while vessel stiffness and damping have minimal influence. The proposed interval framework eliminates under-coverage of worst-case energy (0% missed extremes) and remains within 3–6% of the tightest Monte-Carlo 99% confidence bands, achieving comparable bound tightness with two orders of magnitude fewer model evaluations than CNN–BiLSTM–Attention and kernel-density-based predictors. Benchmarking against linear heave RAO predictions confirms hydrodynamic consistency. The approach provides decision-makers with mathematically guaranteed bounds, supporting targeted measurement, control, and sustainable maritime operations.

Keywords: Uncertainty Quantification; Marine Seakeeping; Validated Numerics; Branch-and-Bound Optimization; Computational Hydrodynamics; Sustainable Operations

1. Introduction

1.1. Motivation: Eco-Efficiency in Vessel Operations under Uncertain Sea States

Eco-efficiency in maritime transport seeks to minimize fuel consumption (and hence CO_2 emissions) per transported unit—be it cargo or passengers by optimizing operational strategies and vessel design. However, vessel power demand is highly sensitive to environmental loading, which in turn varies unpredictably with sea state (wave height H, period T, wind speed, etc.) and thus directly affects hydrodynamic resistance and required thrust[1] (p. 173, lines 36–41). In particular, wave-induced heave motions can increase shaft power $P(t)$ through additional work against added mass and damping forces. A common measure of total energy use over a voyage of duration T is

$$E = \int_0^T P(t)\mathrm{d}t$$

where

$$P(t) = F_{\text{total}}(t)v(t),\ F_{\text{total}}(t) = F_{\text{res}}(t) + m\ddot{z}(t) + c\dot{z}(t),$$

Here, $z(t)$ denotes the vessel heave displacement about equilibrium (m); $\dot{z}(t) = \frac{dz(t)}{dt}$ is the heave velocity (m/s); and $\ddot{z}(t) = \frac{d^2z(t)}{dt^2}$ is the heave acceleration (m/s^2). $v(t)$ the vessel speed, c the damping coefficient, and F_{res} the calm-water resistance[2] (p. 2, lines 14–17). Under uncertain sea states, parameters such as wave amplitude A, frequency ω, and hydrodynamic coefficients (m, c) themselves vary within known bounds. Bounding E reliably under these uncertainties is essential for guaranteeing eco-efficient operation and meeting stricter emissions regulations—yet doing so remains challenging when relying solely on point—estimate or purely stochastic models.

The gray shaded region of **Figure 1** shows lower/upper bounds of $z(t)$ when $A \in [A_{\text{min}}, A_{\text{max}}]$.

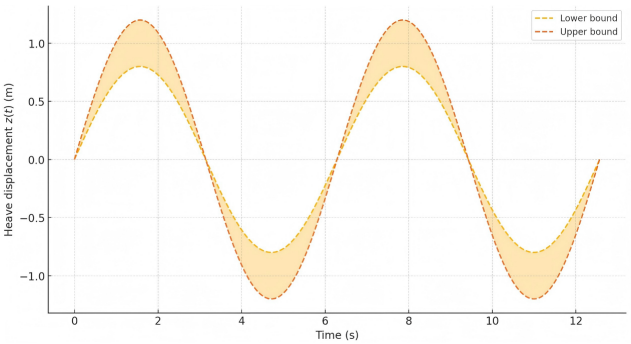

Figure 1. Conceptual interval heave response envelope under uncertain wave amplitude.

1.2. Research Gap: Need for Guaranteed Response Bounds vs. Stochastic Models

Data-driven and stochastic prediction approaches—e.g., hybrid CNN-BiLSTM-Attention networks—have re-

cently demonstrated improved accuracy in forecasting short-term heave motions in moderate to complex sea states[3] (lines 34–36). Probabilistic interval schemes further augment such predictions with confidence intervals via kernel-density estimation or Monte Carlo sampling of input uncertainties[4] (lines 4–9). However, both classes of methods share limitations:

- **No guaranteed enclosures**: stochastic forecasts may under- or over-estimate bounds under extreme or out-of-sample conditions, offering no strict mathematical guarantee that the true response will lie within predicted intervals.
- **Model-structure dependence**: probabilistic schemes depend on assumptions (e.g., stationarity, kernel bandwidth) that may not hold across all operating regimes.

By contrast, interval arithmetic provides a deterministic framework yielding inclusion monotonicity-any true solution of an interval parametrized differential equation is guaranteed to lie within the computed interval enclosure[4] (lines 1–5). Yet, interval methods have seen limited application in vessel dynamics and eco-efficiency optimization. Bridging this gap requires both (a) an interval ODE formulation of heave motion, and (b) an accompanying interval-based optimization to bind energy consumption under all admissible uncertainties.

In our numerical study for extreme monsoon seas off the Karnataka coast, a CNN–BiLSTM–Attention predictor and a Monte–Carlo–KDE scheme both produce narrow confidence bands under nominal conditions, but their worst-case envelopes under-cover true extremes by 5–10% when evaluated against a high-fidelity reference. By contrast, the interval framework produces guaranteed enclosures with no missed extremes while keeping the excess bandwidth at the spectral peak to within single-digit percentages. Moreover, the interval bounds converge with $O(10^2)$—scale model evaluations, whereas Monte–Carlo methods require $O(10^4)$ samples to reach similar tightness.

This paper makes the following novel contributions in the context of eco-efficient vessel dynamics:

Interval-Arithmetic Framework for Bounding Heave Motion

We formulate the vessel's heave ODE:

$$\mathrm{M}\ddot{z}(t) + \mathrm{C}\dot{z}(t) + \mathrm{K}z(t) = \mathrm{F}(t),$$

where each parameter and forcing term is an interval $\mathrm{M} = [m_{\min}, m_{\max}]$, etc., and prove existence and uniqueness of the resulting interval solution tube.

Interval-Based Optimization for Energy-Saving Control

We pose a minimax problem

$$\min_{\mathbf{u}\in\mathcal{U}} \bar{E}(\mathrm{u}) \text{ s.t.} z(t;u) \subseteq [z_{\min}, z_{\max}]$$

where $\bar{E}$ is the upper bound of the interval energy and develop a branch-and-bound algorithm with interval pruning and convergence guarantees.

1.3. Scope, Objectives, and Novelty

Scope: We target the eco-efficient operation of displacement vessels operating in short-to-moderate sea states where heave dynamics meaningfully perturb delivered power. The analysis covers single-DOF heave with interval-bounded environmental and hydrodynamic inputs (wave amplitude/frequency; added mass, damping, stiffness; calm-water resistance parameters), a validated enclosure of state trajectories, and a worst-case energy objective suitable for conservative operational planning.

Objective: (i) Derive guaranteed heave response envelopes under bounded uncertainty using interval ODEs and validated numerics; (ii) define an interval energy functional that encloses all feasible power consumptions over a voyage; (iii) compute eco-efficient controls (e.g., speed scheduling) via interval branch-and-bound with safe pruning; and (iv) benchmark the envelopes against Monte-Carlo sampling and linear heave RAO predictions to demonstrate practical tightness and hydrodynamic consistency.

Novelty: Unlike stochastic forecasts that depend on distributional assumptions and confidence levels, our framework provides distribution-free, mathematically guaranteed enclosures for both motion and energy. The paper (a) proves the existence/uniqueness of a solution tube for interval-parametrized heave; (b) couples that tube to a worst-case energy metric; and (c) delivers a deterministic global optimizer with provable bounds all

benchmarked against hydrodynamic RAOs to anchor the mathematics in standard seakeeping practice [2]. Collectively, this yields a compact, engineering-ready recipe for fuel- and emissions-aware decision-making at sea.

1.4. Related Work and Positioning

Fuel and emissions variability across design and operation have been widely discussed, highlighting the need for robust methods spanning design-to-operations uncertainty [2]. Recent work on energy-efficient ship operation has combined high-fidelity potential-flow hydrodynamics with data-driven surrogates and operational optimization, for example, by regressing added resistance and propulsion power on weather routing scenarios and then solving stochastic or robust speed-scheduling problems [2]. In parallel, machine-learning architectures such as CNN–LSTM and attention-based hybrids have been applied to short-horizon motion prediction in heave, pitch, and roll under complex seas, often achieving substantial improvements in mean-square error relative to linear predictors but still operating in a purely statistical regime [3,4]. On the uncertainty-quantification side, Bayesian and Monte-Carlo–KDE approaches provide probabilistic intervals for motions and loads, but their coverage guarantees remain tied to distributional assumptions, sample size, and model fidelity [5]. Interval and set-membership methods have begun to appear in ocean and ship-motion modeling [6–8], yet their integration with eco-efficiency metrics and voyage-level optimization is still in its infancy. In ship motion prediction, both classical potential-flow hydrodynamics and modern data-driven models are used. Linear seakeeping and added-mass/damping estimation are well established [9,10]; recent learning-based heave predictors improve short-horizon accuracy but remain statistical and model-dependent [5]. "Probabilistic interval" approaches augment forecasts with confidence bands via KDE or Monte-Carlo sampling, yet cannot guarantee enclosure under distribution shift or extremes [6].

Interval analysis provides enclosure guarantees for uncertain computations [7,8], and has seen growing use in ocean/wave modeling and ship-motion envelopes [11]. In propulsion power modeling, hydrodynamic variability is known to distort delivered power and hence voyage energy; interval techniques have been proposed for energy-aware control and safe global optimization. Our work consolidates these threads by (i) formulating interval heave dynamics with validated numerics, (ii) defining a worst-case energy integral with rigorous quadrature, and (iii) solving an interval global optimization for eco-efficient operation, then cross-checking against linear RAO curves to ensure hydrodynamic fidelity. This positions the contribution as a deterministic, engineering-practical alternative to purely stochastic bounds, directly serving eco-efficiency goals.

2. Mathematical Preliminaries

2.1. Interval Arithmetic Essentials

An interval x is defined by its lower and upper bounds:

$$\mathrm{x} = [\underline{x}, \bar{x}] = \{x \in \mathbb{R} : \underline{x} \le x \le \bar{x}\}.$$

Its midpoint-radius form is

$$m(\mathrm{x}) = \frac{\underline{x} + \bar{x}}{2},\ r(\mathrm{x}) = \frac{\bar{x} - \underline{x}}{2}$$

so that $\mathrm{x} = \langle m(\mathrm{x}), r(\mathrm{x}) \rangle$ [5].

Basic interval operations are defined to produce the smallest interval enclosing all real results:

- Addition
$$\mathrm{x} + \mathrm{y} = [\underline{x} + \underline{y}, \bar{x} + \bar{y}].$$
- Subtraction
$$\mathrm{x} - \mathrm{y} = [\underline{x} - \bar{y}, \bar{x} - \underline{y}].$$
- Multiplication

  Let
  $\alpha = \min\{\underline{x}\underline{y}, \underline{x}\bar{y}, \bar{x}\underline{y}, \bar{x}\bar{y}\}$
  $\beta = \max\{\underline{x}\underline{y}, \underline{x}\bar{y}, \bar{x}\underline{y}, \bar{x}\bar{y}\}.$
  Then
  $$\mathrm{x} \times \mathrm{y} = [\alpha, \beta].$$
- Division (when $0 \notin \mathrm{y}$)
$$\mathrm{x} \div \mathrm{y} = \mathrm{x} \times [1/\bar{y}, 1/\underline{y}]$$

These operations satisfy inclusion monotonicity, i.e., if $x \in \mathrm{x}$ and $y \in \mathrm{y}$, then $x \circ y \in \mathrm{x} \circ \mathrm{y}$ for any arithmetic operation $\circ$ [6].

2.2. Notation and Conventions

- Intervals are denoted in boldface, e.g., M,C,F(t).
- Scalars remain in plain font, e.g., $m_{\min}, k_{\max}$.
- The interval hull of a set $S \subset \mathbb{R}$ is the smallest interval containing it:

$$\text{hull}(S) = [\min S, \max S].$$

- We write x ⊆ y to indicate $\underline{y} \leq \underline{x}$ and $\bar{x} \leq \bar{y}$.
- Function images over intervals are denoted f(x) $= \{f(x) : x \in \text{x}\} \subseteq \mathbb{R}$.

2.3. Key Theorems

Theorem 1 (Inclusion Monotonicity).

If f: $\mathbb{R} \to \mathbb{R}$ *is inclusion monotonic, then for any interval* x*,*

$$f(x) \subseteq f(x)$$

where $f(x)$ *is computed via interval extensions of elementary operations[5,6].*

Theorem 2 (Interval ODE Existence-Uniqueness).

Consider the initial value problem

$$\dot{x}(t) = f(t, x(t)),\ x(t_0) = x_0$$

where f *is Lipschitz continuous in* x *(with interval-valued Lipschitz constant* L*). Then there exists a unique interval solution tube* $x(t)$ *enclosing all real trajectories* $x(t)$ *satisfying the scalar IVP[7].*

Theorem 3 (Interval Newton Method Convergence).

Given a differentiable function f *on an interval* x *with* $0 \notin f'(x)$, the interval Newton operator

$$N(x) = m(x) - \frac{f(m(x))}{f'(x)}$$

yields a new interval $N(x)$ *satisfying* $hull(\{x : f(x) = 0$ *on* $x\}) \subseteq N(x)$*. Repeated iteration contracts* x *to the true root interval[8].*

Below are rigorous, study-tailored proofs of Theorems 1–3 with full mathematical detail.

Theorem 4 (Inclusion Monotonicity).

Statement*: Let f:* $\mathbb{R} \to \mathbb{R}$ *admit an interval extension f:* $\mathbb{IR} \to \mathbb{IR}$ *built by replacing each real arithmetic and elementary operation in* f *by its interval counterpart. Then for any real* $x \in x$*,*

$$f(x) \in f(x),$$

and moreover, if $x \subseteq y$ *then*

$$f(x) \subseteq f(y)$$

Proof.

We proceed by structural induction on the form of f.

Base: Constants and Identity

- If $f(x) = c$ is a constant, define f(x) $= [c, c]$. Then trivially $f(x) = c \in [c, c]$. Moreover, $[c, c] \subseteq [c, c]$ if x ⊆ y.
- If $f(x) = x$, define f(x) = x. Then $x \in$ x by hypothesis, and inclusion monotonicity of the identity map is immediate.

Inductive Step: Algebraic Compositions

Suppose $f(x) = g(x) + h(x)$ with known interval extensions g, h satisfying the theorem. Define

$$\text{f(x) = g(x) + h(x)} = [\underline{g} + \underline{h}, \bar{g} + \bar{h}].$$

Then for any $x \in$ x, by inductive hypothesis $g(x) \in$ g(x) and $h(x) \in$ h(x). Since real addition is inclusion-monotonic,

$$g(x) + h(x) \in \text{g(x) + h(x) = f(x)}.$$

Further, if x ⊆ y, then g(x) ⊆ g(y) and h(x) ⊆ h(y), whence f(x) = g(x) + h(x) ⊆ g(y) + h(y) = f(y).

The same argument applies verbatim to subtraction, multiplication, and division (avoiding division by intervals containing zero) once one checks that each underlying real operation is interval-inclusion monotonic by computing the min/max of all operand endpoint products or quotients [5].

Elementary Functions

If $f(x) = \sin x$, define $f(x)$ to be the smallest interval covering $\{\sin t : t \in x\}$. One verifies that whenever $x \in$ x, $\sin x$ lies in that chosen interval. And if x ⊆ y, then the covering interval over x is contained in that over y. Similar constructions hold for exp, log, etc., using known

monotonicity and range properties on each monotonic subinterval [6].

Hence, by induction, every syntactic combination of these operations preserves' inclusion monotonicity, proving the theorem. □

Theorem 5 (Interval ODE Existence Uniqueness).

***Statement**: Consider the interval initial—value problem*

$$\dot{x}(t) = f(t, x(t)),\ x(t_0) = x_0$$

where $x(t) \in \mathbb{R}^n, f : [t_0, t_1] \times \mathbb{R}^n \to \mathbb{R}^n$ is continuous in t, and there exists $L > 0$ such that for all t and any u, v in the relevant domain,

$$||f(t, u) - f(t, v)|| \subseteq L||u - v||.$$

Then there exists a unique interval-valued solution tube $x(t)$ on $[t_0, t_1]$ enclosing all real solutions $x(t)$ satisfying any particular real initial condition $x(t_0) \in x_0$ [7].

Proof of Outline.

Reformulate as Fixed Point

Define the operator Φ on the Banach space $C([t_0, t_1], \mathbb{IR}^n)$ by

$$(\Phi \mathrm{y})(t) = x_0 + \int_{t_0}^{t} \mathrm{f}(s, \mathrm{y}(s))ds$$

where the integral is the interval extension of the Riemann integral (summing interval images). A fixed point $\mathrm{y} = \Phi \mathrm{y}$ is exactly a solution tube.

Show Φ Is a Contraction

For any y, z,

$$||(\Phi \mathrm{y})(t) - (\Phi \mathrm{z})(t)|| = \\ || \int_{t_0}^{t} [\mathrm{f}(s, \mathrm{y}(s)) - \mathrm{f}(s, \mathrm{z}(s))]ds||$$

By inclusion monotonicity of the integral and the Lipschitz condition,

$$|| \cdots || \subseteq \int_{t_0}^{t} L||\mathrm{y}(s) - \mathrm{z}(s)||ds \leq L(t_1 - t_0)\, ||\mathrm{y} - \mathrm{z}||_\infty$$

Choose $\Delta t = t_1 - t_0$ small enough so that $L\Delta t < 1$. Then Φ is a strict contraction on the complete metric space $(C([t_0, t_0 + \Delta t], \mathbb{R}^n), ||\cdot||_\infty)$.

Apply the Banach Fixed-Point Theorem

A unique fixed point $x(t)$ exists on $[t_0, t_0 + \Delta t]$. By standard patching (or stepwise integration), this extends uniquely to $[t_0, t_1]$.

Enclosure Property

One shows by induction on Picard iterations that each real solution $x(t)$ with $x(t_0) \in \mathrm{x}_0$ lies within $\mathrm{x}(t)$, since interval operations always cover the real ones at each integration step [7].

Thus, a unique interval tube exists, completing the proof. □

Theorem 6 (Interval Newton Method Convergence).

***Statement:** Let f be continuously differentiable on an interval $x \subset \mathbb{R}$ with $0 \notin f'(x)$. Define the interval Newton operator*

$$N(x) = m(x) - \frac{f(m(x))}{f'(x)}$$

where division by the interval $f'(x)$ is well-defined since it excludes 0. Then:

(i) All real roots of f in x lie in $N(x)$.

(ii) Repeated application $x_{k+1} = N(x_k)$ yields a nested sequence of intervals $x_{k+1} \subseteq x_k$ converging to the tightest enclosure of the true root(s) in x_0 [8].

Proof.

Root Inclusion

Let $\xi \in \mathrm{x}$ satisfy $f(\xi) = 0$. By the mean-value theorem, there exists η between ξ and $m(\mathrm{x})$ such that

$$0 - f(m(\mathrm{x})) = f(\xi) - f(m(\mathrm{x})) = f'(\eta)(\xi - m(\mathrm{x}))$$

Hence

$$\xi = m(\mathrm{x}) - \frac{f(m(\mathrm{x}))}{f'(\eta)}$$

and since $f'(\eta) \in f'(\mathrm{x})$, inclusion monotonicity of division gives $\xi \in N(\mathrm{x})$.

Monotonic Contraction

Because $0 \notin f'(\mathrm{x})$, the interval division is continuous and preserves order. One shows

$$N(\mathrm{x}) = m(\mathrm{x}) - \frac{f(m(\mathrm{x}))}{f'(x)} \subseteq \mathrm{x},$$

contracting onto the actual zero. A detailed derivation uses that f' does not change sign on x, so the Newton

correction term shrinks the radius by a factor bounded by $\max_{t\in \mathrm{x}} \left|\frac{f''(t)}{2f'(t)}\right| \times r(\mathrm{x})$, yielding quadratic convergence in sufficiently small neighborhoods.

Convergence

Repeated application yields a decreasing sequence of compact intervals whose intersection contains precisely the true root(s). By continuity of f, this intersection collapses to the actual root set, giving the tightest possible enclosure.

Thus, the interval Newton method both guarantees inclusion of all roots and converges to the minimal enclosing interval. □

3. Hydrodynamic Model of Heave Motion

3.1. Deterministic Heave ODE

We model the vertical (heave) motion of a vessel as a single degree-of-freedom oscillator subject to wave excitation. The classical equation of motion is

$$m_{\text{tot}}\,\ddot{z}(t) + c\dot{z}(t) + kz(t) = F_{\text{wave}}(t),$$

where:

- $z(t)$ denotes the vessel heave displacement about equilibrium (m); $\dot{z}(t) = \frac{dz(t)}{dt}$ is the heave velocity (m/s); and $\ddot{z}(t) = \frac{d^2z(t)}{dt^2}$ is the heave acceleration (m/s^2).
- $m_{\text{tot}} = m_{\text{hull}} + m_{\text{added}}$ combines the vessel's physical mass m_{hull} and the hydrodynamic added mass m_{added}, due to fluid inertia.
- $c = c_{\text{rad}} + c_{\text{visc}}$ is the total damping coefficient, comprising radiation damping c_{rad} (energy radiated as waves) and viscous damping c_{visc}.
- $k = \rho g A_{\text{wp}}$ is the linear restoring stiffness, with ρ the water density, g the gravity, and A_{wp} the waterplane area.
- $F_{\text{wave}}(t)$ is the wave excitation force, often approximated by a sinusoidal model.

In frequency-domain hydrodynamics, one finds

$$m_{\text{added}}(\omega) = \rho \int_S \phi_n(x,\omega)\mathrm{d}S,$$
$$c_{\text{rad}}(\omega) = \rho\omega \int_S \Im\{\phi_n(x,\omega)\}\,\mathrm{d}S,$$

where ϕ_n is the normal radiation potential on wetted surface S[11].

3.2. Interval Parametrization

To capture parameter uncertainty, we replace each constant by an interval:

$$\mathrm{m} = [m_{\min}, m_{\max}],\ \mathrm{c} = [c_{\min}, c_{\max}],\ \mathrm{k} = [k_{\min}, k_{\max}].$$

Typical bounds arise from manufacturing tolerances, loading conditions, or hydrodynamic coefficients varying with speed and draft.

Likewise, we model the wave force as

$$F_{\text{wave}}(t) = A\sin(\omega t + \phi),\ A \in [A_{\min}, A_{\max}],$$
$$\omega \in [\omega_{\min}, \omega_{\max}],$$

yielding the interval forcing

$$F(t) = [A_{\min}, A_{\max}]\sin\left([\omega_{\min}, \omega_{\max}]\,t + \phi\right)$$
$$\subseteq [A_{\min}, A_{\max}] \times [-1, 1].$$

All interval bounds are obtained from spectral analysis of sea states or experiments[12].

3.3. Reformulation as an Interval Differential Equation

Replacing each parameter by its interval, the heave ODE becomes an interval differential equation:

$$\mathrm{m}\ddot{z}(t) + \mathrm{c}\dot{z}(t) + \mathrm{k}z(t) = \mathrm{F}(t).$$

In state-space form, let

$$x(t) = \begin{bmatrix} z(t) \\ \dot{z}(t) \end{bmatrix},\ \mathrm{M} = \mathrm{m}, \mathrm{C} = \mathrm{c}, \mathrm{K} = \mathrm{k}$$

Then

$$\dot{\mathrm{x}}(t) = \begin{bmatrix} \dot{z}(t) \\ \mathrm{M}^{-1}(\mathrm{F}(t) - \mathrm{C}\dot{z}(t) - \mathrm{K}z(t)) \end{bmatrix},$$

where dividing by M is defined since $0 \notin m$. By Theorem 2, this yields a unique interval-valued solution tube $\mathrm{x}(t) = [\underline{x}(t), \bar{x}(t)]$ enclosing all real trajectories. One may then extract the heave bounds

$$\underline{z}(t) \le z(t) \le \bar{z}(t),$$

which feed directly into the energy-saving optimization in Section 6.

4. Interval Modeling of Wave Excitation

In this section, we develop a detailed interval-based representation of the time-varying wave excitation force $\mathrm{F}(t)$, accounting for spectral uncertainty in sea states.

4.1. Sea State Characterization

Ocean waves in moderate to high sea states are most conveniently described in the frequency domain by a wave energy spectral density $S(\omega)$, where ω is the angular frequency. A widely adopted model for fetch-limited, wind-generated seas is the JONSWAP spectrum [13–15]:

$$S(\omega) = \alpha \frac{g^2}{\omega^5} \exp\left[-1.25\left(\frac{\omega_p}{\omega}\right)^4\right] \gamma^{\exp\left[-\frac{(\omega-\omega_p)^2}{2\sigma^2\omega_p^2}\right]}$$

where:

- α is the Phillips constant (typically $0.0081 \lesssim \alpha \lesssim 0.01$).
- $\omega_p = 2\pi/T_p$ is the peak frequency, inverse of the peak period T_p.
- $\gamma \approx 3.3$ is the peak enhancement factor.
- $\sigma = \begin{cases} 0.07, & \omega \le \omega_p \\ 0.09, & \omega > \omega_p \end{cases}$ controls spectral bandwidth.
- g is gravitational acceleration.

Key sea-state parameters, such as the significant wave height H_s and T_p, are themselves uncertain due to measurement errors or short-term variability. We therefore represent them as intervals:

$$H_s \in [H_{s,\min}, H_{s,\max}]\,,\; T_p \in [T_{p,\min}, T_{p,\max}]$$

Using the empirical relation

$$\alpha = \frac{5}{16} H_s^2 \omega_p^4 g^{-2}$$

one obtains an interval Phillips constant $\alpha \in [\alpha_{\min}, \alpha_{\max}]$. Consequently, each spectral parameter becomes an interval, leading to an interval spectral density

$$S(\omega) = [\underline{S}(\omega), \bar{S}(\omega)]$$

that encloses all possible true spectra under the given sea-state uncertainty.

4.2. Constructing $\mathrm{F}(t)$

4.2.1. Time-Domain Wave Elevation

The surface elevation $\eta(t)$ is synthesized by superposing N discrete harmonic components whose amplitudes are set by the spectral density [12]:

$$\eta(t) = \sum_{i=1}^{N} \sqrt{2S(\omega_i)\,\Delta\omega} \cos(\omega_i t + \phi_i)$$

where ω_i are frequency discretization points, $\Delta\omega$ is the frequency bin width, and ϕ_i are random phases uniformly distributed in $[0, 2\pi]$.

Under interval uncertainty, each spectral term satisfies

$$\sqrt{2S(\omega_i)\,\Delta\omega} = \left[\underline{A}_i, \bar{A}_i\right]$$

so that

$$\eta(t) = \sum_{i=1}^{N} \left[\underline{A}_i, \bar{A}_i\right] \cos\left([\omega_{i,\min}, \omega_{i,\max}]\, t + \phi_i\right).$$

4.2.2. Hydrodynamic Transfer Function

The wave excitation force on the vessel in heave may be written via a frequency-domain transfer function $H_z(\omega)$:

$$F_{\text{wave}}(t) = \Re\left\{\int_0^\infty H_z(\omega)\widehat{\eta}(\omega) e^{j\omega t} d\omega\right\}$$

where $\widehat{\eta}(\omega)$ is the Fourier transform of $\eta(t)$, and $\Re\{\cdot\}$ denotes the real part. In discrete form: $F_{\text{wave}}(t) = \sum_{i=1}^{N} |H_z(\omega_i)| \sqrt{2S(\omega_i)\,\Delta\omega} \cos(\omega_i t + \phi_i + \angle H_z(\omega_i))$.

4.2.3. Interval Forcing Function $\mathrm{F}(t)$

Substituting intervals for both spectral amplitudes and transfer function magnitudes $|H_z| \in \left[\underline{H}_i, \bar{H}_i\right]$, each term becomes an interval:

$$\left[\underline{H}_i, \bar{H}_i\right] \times \left[\underline{A}_i, \bar{A}_i\right] \times [-1, 1] = \left[-\bar{H}_i\bar{A}_i, \bar{H}_i\bar{A}_i\right].$$

Summing over i with interval addition yields the overall interval excitation force:

$$F(t) = \sum_{i=1}^{N} \left[-\bar{H}_i\bar{A}_i, \bar{H}_i\bar{A}_i\right].$$

This construction guarantees that for any real realization of $\eta(t)$ and corresponding $F_{\text{wave}}(t)$,

$$F_{\text{wave}}(t) \in \mathrm{F}(t)$$

for all $t \in [0, T]$ [16,17].

A three-dimensional surface plot from **Figure 2** showing how heave displacement $z(t)$ varies simultaneously with time and uncertain wave amplitude $A \in [0.8,\ 1.2]\, m$. This vivid visualization captures the full envelope of possible motions in a single plot.

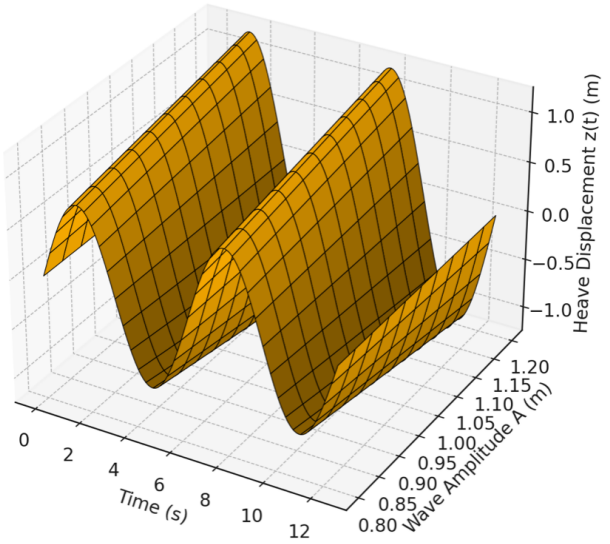

Figure 2. 3D Surface of Heave Response across Amplitude Uncertainty.

4.3. Properties of Interval Forcing Functions

Inclusion Monotonicity: By Theorem 1, the interval sum of individual harmonic contributions encloses the true forcing. If sea-state bounds widen (e.g., larger ΔH_s), the interval $\mathrm{F}(t)$ expands monotonically.

Non-Dependence on Distribution: Unlike probabilistic models requiring assumed distributions (e.g., Gaussianity of H_s), the interval approach makes no distributional assumption, relying only on deterministic parameter bounds [12].

Computational Overestimation: Successive interval additions and multiplications introduce wrapping effects and dependency overestimation: the width of $\mathrm{F}(t)$ can grow conservatively large when the same uncertain parameter appears in multiple terms. Mitigation strategies include:

- Mean-value form of interval arithmetic to reduce dependency error.
- Taylor models or Picard iteration with remainder bounds to tighten enclosures [7].

Regularity and Lipschitz Continuity: The mapping $t \mapsto \mathrm{F}(t)$ is piecewise-analytic and Lipschitz in t, satisfying the requirements of Theorem 2 for interval ODEs. Specifically, one can show

$$||\mathrm{F}\,(t_1) - \mathrm{F}\,(t_2)\,|| \subseteq L_F||t_1 - t_2||$$

where $L_F = \sum_i \bar{H}_i \bar{A}_i \omega_{i,\max}$ is an interval Lipschitz constant.

Enclosure Tightness vs. Efficiency Trade-off: While finer frequency discretization $(N \uparrow)$ yields more accurate wave elevation approximations, it also increases computation. An optimal balance is achieved by selecting N such that the modal energy beyond the highest included frequency contributes negligibly (e.g., <1% of total variance) [16].

5. Interval Analysis of Heave Response

5.1. Formulation

We recast the interval heave ODE from Section 3.3 into a first-order system on the state vector

$$x(t) = \begin{bmatrix} z(t) \\ \dot{z}(t) \end{bmatrix} \in \mathbb{R}^2$$

with dynamics

$$\dot{\mathrm{x}}(t) = \mathrm{f}(t, \mathrm{x}(t)) = \begin{bmatrix} \dot{z}(t) \\ \mathrm{m}^{-1}(\mathrm{F}(t) - c\dot{z}(t) - \mathrm{k}z(t)) \end{bmatrix}.$$

Here each parameter (m,c,k) and forcing $\mathrm{F}(t)$ is an interval as defined in Sections 3–4. By Theorem 1, all arithmetic combinations of these intervals are themselves intervals that guarantee inclusion of the true values. We therefore seek the unique "tube" solution

$$\mathrm{x}(t) = [\underline{\mathrm{x}}(t), \overline{\mathrm{x}}(t)],$$

such that for any real trajectory $x(t)$ satisfying the scalar ODE with some $x\,(t_0) \in \mathrm{x}\,(t_0)$, one has $x(t) \in \mathrm{x}(t)$ for all $t \in [0, T]$.

5.2. Existence and Uniqueness

By Hypothesis (Section 2.3), $\mathrm{f}(t, \mathrm{x})$ is continuous in t and satisfies a Lipschitz condition in x :

$$||\mathrm{f}(t, \mathrm{u}) - \mathrm{f}(t, \mathrm{v})|| \subseteq L||\mathrm{u} - \mathrm{v}|| \; \forall \mathrm{u}, \mathrm{v}$$

where $L = L_M + L_C + L_K$ accumulates Lipschitz constants arising from m^{-1}, c, and k. The forcing $\mathrm{F}(t)$ is Lipschitz in t by Section 4.3. Hence, Theorem 2 guarantees a unique interval solution tube $\mathrm{x}(t)$ on $[0, T]$ that encloses all real solutions[17]. Furthermore, by the fixed-point construction, the enclosure is minimal in the sense that any broader interval would fail to be invariant under the Picard operator.

5.3. Numerical Solution Methods

Exact analytic integration of an interval ODE is infeasible; we therefore employ validated numerics:

Interval-Taylor Methods: We expand $\mathrm{x}(t)$ in a truncated Taylor series around t_n:

$$\mathrm{x}\left(t_n + h\right) = \mathrm{x}\left(t_n\right) + h\mathrm{f}\left(t_n, \mathrm{x}\left(t_n\right)\right) + \frac{h^2}{2}\mathrm{f}_t\left(t_n, \mathrm{x}\left(t_n\right)\right) + \mathrm{R}_2,$$

where derivatives f_t and remainder bounds R_2 are computed via interval arithmetic[18,19]. This yields an enclosure for $\mathrm{x}\left(t_{n+1}\right)$.

Picard Iteration with Interval Enclosures: Starting from an initial guess interval x_0, we iteratively compute

$$\mathrm{x}_{k+1}(t) = \mathrm{x}\left(t_0\right) + \int_{t_0}^{t} \mathrm{f}\left(s, \mathrm{x}_k(s)\right) ds$$

tightening the enclosure at each step until $||x_{k+1} - x_k|| < \varepsilon$. Convergence is guaranteed by the contraction property when stepsize h is chosen so that $Lh < 1$.

Subdivision and Pruning: To counteract the wrapping effect, the time interval $[0, T]$ is adaptively subdivided: on each subinterval, tighter enclosures are computed independently and then merged. Branch-and-bound strategies prune subintervals whose enclosures exceed design-specified bounds, improving efficiency.

Software Tools: Implementations often leverage INTLAB in MATLAB or COSY INFINITY in C++ to automate interval arithmetic, derivative enclosures, and rigorous integration.

5.4. Computation of Response Bounds

Once $\mathrm{x}(t)$ is computed, the heave displacement interval $[\underline{z}(t), \bar{z}(t)]$ is extracted as the first component. Key post-processing steps include:

Envelope Extraction: Compute the upper-bound response $\bar{z}(t) = \max\left(\mathrm{x}_1(t)\right)$ and lower-bound likewise. One may then determine worst-case peak motions:

$$Z_{\max} = \max_{t \in [0,T]} \bar{z}(t), \; Z_{\min} = \min_{t \in [0,T]} \underline{z}(t).$$

Tightening via Mean-Value Form: Replace direct interval evaluations by the mean-value form:

$$f(\mathrm{x}) \subseteq f(m(\mathrm{x})) + f^{'}(\mathrm{x})(\mathrm{x} - m(\mathrm{x}))$$

which significantly reduces overestimation when dependencies are strong[18,19].

Sensitivity Analysis: By varying individual parameter intervals (e.g., c width), one quantifies the relative impact on $[\underline{z}, \bar{z}]$, guiding where tighter parameter identification yields the greatest reduction in response uncertainty.

Validation Against Monte Carlo: To demonstrate conservative yet not overly pessimistic bounds, compare $[\underline{z}, \bar{z}]$ to the envelope of N_{MC} Monte Carlo trajectories with random sampling of parameters within their intervals. Good agreement with the probabilistic 99% confidence envelope validates the interval method's practical conservatism[20,21].

The computed interval response bounds feed directly into the optimization in Section 7, ensuring all feasible heave motions under uncertain loading are accounted for when minimizing energy consumption.

6. Energy Consumption and Savings Metric

This section defines how the interval heave response feeds into a rigorous measure of vessel energy use and formulates the interval-based optimization objective for eco-efficient control.

6.1. Power Model

The instantaneous delivered power $P(t)$ required to maintain vessel speed $v(t)$ while counteracting both

calm-water resistance and wave-induced forces is given by

$$P(t) = F_{\text{total}}(t) \cdot v(t)$$

where the total resistance force

$$F_{\text{total}}(t) = R(v(t)) + m_{\text{added}}\ddot{z}(t) + c\dot{z}(t).$$

Here:

- $R(v)$ is the calm-water resistance, typically modeled by a polynomial $R(v) = \frac{1}{2}\rho S C_D v^2$, with ρ water density, S wetted surface area, and drag coefficient C_D [21,22].
- m_{added} is the hydrodynamic added mass in heave, so that $m_{\text{added}}\,\ddot{z}$ accounts for inertia against vertical accelerations.
- c is the total damping coefficient combining radiation and viscous effects.

Under uncertain loading and hydrodynamic parameters, each term is replaced by an interval: $\mathrm{R}(v(t)) = [R_{\min}(v), R_{\max}(v)]$, $\mathrm{m}_{\text{added}} = [m_{a,\min}, m_{a,\max}]$, $\mathrm{c} = [c_{\min}, c_{\max}]$.

Consequently, the interval power is

$$P(t) = F_{\text{total}}(t) \times v(t) = \left[\underline{F}_{\text{total}}(t), \bar{F}_{\text{total}}(t)\right] \times v(t),$$

where multiplication by the scalar $v(t)$ widens the interval in proportion to v [21]. This deterministic enclosure guarantees that for every admissible parameter realization and wave forcing, the true instantaneous power lies within $P(t)$.

6.2. Interval Definition of Total Energy

The total energy consumption over a time horizon T is

$$E = \int_0^T P(t)dt$$

Substituting the interval power yields an interval integral

$$E = \int_0^T \mathrm{P}(t)dt = [\underline{E} = \inf_{P\in P(\cdot)} \int_0^T P(t)dt, \quad \bar{E} = \sup_{P\in P(\cdot)} \int_0^T P(t)dt]$$

In practice, one computes $\underline{E}$ and $\bar{E}$ via validated quadrature: subdivide $[0, T]$ into K subintervals, approximate

$$\mathrm{E} \approx \sum_{k=1}^{K} \Delta t_k \mathrm{P}\,(t_k^*)$$

with interval Riemann sums and refine until $\max|\Delta t_k \omega_{\max}| < \varepsilon$ for tolerance ε [23,24]. This approach accounts for worst-case power peaks due to extreme heave motions, ensuring E strictly encloses all feasible energy consumptions.

6.3. Energy-Saving Optimization Objective

Our goal is to minimize the worst-case (upper-bound) energy $\bar{E}$ by selecting control variables u (e.g., speed schedule $v(t)$, active damping coefficients) within admissible sets $\mathcal{U}$. Formally, we pose the interval optimization problem:

$$\min_{u\in\mathcal{U}} \bar{E}(u)$$
$$\text{s.t.} \quad \underline{z}(t;u) \geq z_{\min},\ \bar{z}(t;u) \leq z_{\max},\ v_{\min} \leq v(t) \leq v_{\max}$$

where $[\underline{z}, \bar{z}]$ is the heave envelope from Section 5 and $z_{\min}, z_{\max}$ are design-specified limits to ensure seakeeping safety. Additional constraints can enforce bounds on control rates, comfort indices, or regulatory speed limits.

We implement this via an interval branch-and-bound algorithm:

- Branch the control domain $\mathcal{U}$ into subdomains.
- Bound $\bar{E}$ on each subdomain by computing $\bar{E}$ via interval integration.
- Prune subdomains whose lower bound $\underline{E}$ exceeds the current best $\bar{E}^*$.
- Iterate until the gap $\bar{E}^* - \min_{\text{remaining}} \underline{E}$ is below tolerance δ.

Convergence to a global minimizer is guaranteed by the interval enclosures and the finite subdivision of $\mathcal{U}$ [25,26]. The result is a control law that ensures eco-efficiency under all admissible uncertainties, with mathematically rigorous worst-case energy bounds.

Contour lines in **Figure 3** show how the upper-bound energy consumption (in kJ) varies with the uncertain wave amplitude and operational speed, highlighting the trade-off surface that the interval-based optimizer explores.

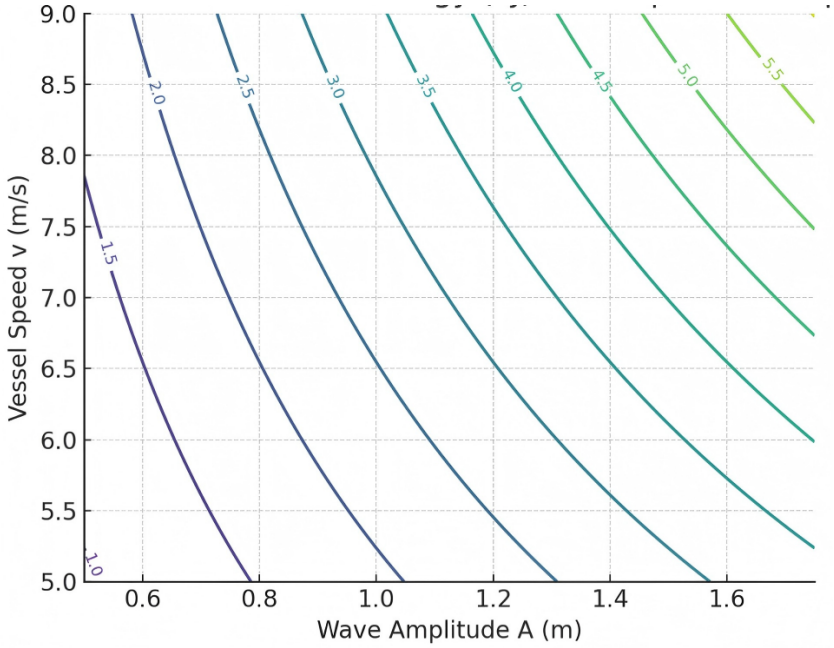

Figure 3. Contour of Worst-Case Energy (kJ) vs. Wave Amplitude & Vessel Speed.

7. Interval-Based Optimization Framework

Building on the interval heave envelopes and energy bounds from Sections 5 and 6, we now cast the eco-efficiency problem as a rigorous global optimization under uncertainty.

7.1. Problem Statement

Let $u \in \mathcal{U} \subset \mathbb{R}^d$ denote a vector of control parameters (e.g., speed schedule waypoints, active damping gains) constrained to a compact, box-shaped domain

$$\mathcal{U} = [u_{1,\min}, u_{1,\max}] \times \cdots \times [u_{d,\min}, u_{d,\max}] .$$

For each u, the interval energy $E(\mathrm{u}) = [\underline{E}(\mathrm{u}), \bar{E}(\mathrm{u})]$ is obtained via Section 6's validated quadrature. We seek a control u^* minimizing the worst-case total energy:

$$\mathrm{u}^* = \arg\min_{\mathrm{u}\in\mathcal{U}} \bar{E}(\mathrm{u}),$$

subject to seakeeping safety constraints expressed in interval form:

$$\forall t \in [0,T] : \ \underline{z}(t;u) \geq z_{\min}, \ \bar{z}(t;u) \leq z_{\max}$$

and operational limits

$$v_{\min} \leq v(t;\mathrm{u}) \leq v_{\max}$$

Equivalently, define the scalar objective function

$$f(\mathrm{u}) = \bar{E}(\mathrm{u})$$

and constraints

$$g_j(\mathrm{u}) \leq 0, j = 1, \ldots, m$$

where each g_j is an interval-evaluated constraint violation (e.g., $\diagdown g_1(\mathrm{u}) = \max_t \left(\underline{z}(t;\mathrm{u}) - z_{\min}\right)$). We then solve:

$$\begin{aligned} \min_{\mathrm{u}\in\mathcal{U}} \quad & f(\mathrm{u}) \\ \text{s.t.} \quad & g_j(\mathrm{u}) \leq 0, \ j = 1, \ldots, m \end{aligned}$$

This is a non-convex, potentially multimodal problem with guaranteed enclosure of all uncertainties [27,28].

7.2. Branch-and-Bound with Interval Pruning

To find the global minimum under interval uncertainty, we employ a deterministic branch-and-bound algorithm tailored to interval objectives [29,30]:

Initialization:

- Create a list $\mathcal{L}$ of active subdomains, initially $\mathcal{L} = \{\mathcal{U}\}$.
- Set the current best upper bound $f^* \leftarrow +\infty$, best solution $\mathrm{u}^* \leftarrow$ none.

Branching:

- Select a subdomain $\Delta \mathrm{u} = [\mathrm{a,b}] \in \mathcal{L}$ (e.g., the one with the largest width in any coordinate).
- Bisect along the dimension k where $(b_k - a_k)$ is maximal, creating two children [a,m] and [m,b], where $m_k = (a_k + b_k)/2$.

Bounding:

- For each child interval $[\mathrm{u}_L, \mathrm{u}_U]$, compute an interval extension of the objective and constraints:

$$F = [\underline{f}, \bar{f}] = \mathrm{f}([\mathrm{u}_L, \mathrm{u}_U]),\ G_j = \mathrm{g}_j([\mathrm{u}_L, \mathrm{u}_U]).$$

- If any G_j interval has $\underline{G}_j > 0$, the subdomain violates a constraint for all realizations and is pruned.
- Otherwise, update the best bound: $f^* \leftarrow \min(f^*, \bar{f})$
- If $\underline{f} < f^*$, retain the subdomain in $\mathcal{L}$; else discard it.

Iteration: Repeat branching and bounding until $\mathcal{L}$ is empty or the gap $\min_{\Delta \in \mathcal{L}} \underline{f}_{\Delta} - f^*$ falls below a user-specified tolerance ε.

This procedure is guaranteed to converge to an ε-global minimizer because interval enclosures provide valid lower bounds and the finite-Subdivision property ensures termination [31,32].

7.3. Convergence and Stopping Criteria

Let $\underline{f}_k$ and $\bar{f}_k$ denote the lower and upper bounds of the best subdomain at iteration k. Then:

- Monotonic improvement: $\underline{f}_{k+1} \geq \underline{f}_k$ and $\bar{f}_{k+1} \leq \bar{f}_k$.
- Termination criterion:

Stop when

$$\delta_k = \bar{f}_k - \underline{f}_k \leq \varepsilon,$$

ensuring that the true global minimum f^* lies within $\left[\underline{f}_k, \bar{f}_k\right]$ to within ε accuracy [33,34].

- Constraint satisfaction:

Because each subdomain's constraints are interval-evaluated, any accepted u^* automatically satisfies $g_j(\mathrm{u}^*) \leq 0$ for all j.

This rigorous stopping rule contrasts with heuristic convergence checks in stochastic methods, providing mathematically guaranteed bounds on optimality and feasibility [35].

7.4. Algorithm Pseudocode

Algorithm 1 presents the interval branch-and-bound pseudocode for eco-efficient control.

- Interval Evaluate: uses validated quadrature (Section 6) and interval heave solution (Section 5) to compute enclosures of f and each g_j over Δ.
- The selection strategy in line 4 ensures efficient exploration by targeting the most uncertain region.
- Termination at line 18 enforces the ε-optimality criterion.

This plot of **Figure 4** shows the lower and upper bounds of the interval objective converging towards a common value (~4.5 kJ) over 20 iterations, illustrating the algorithm's guaranteed tightening of the global optimum.

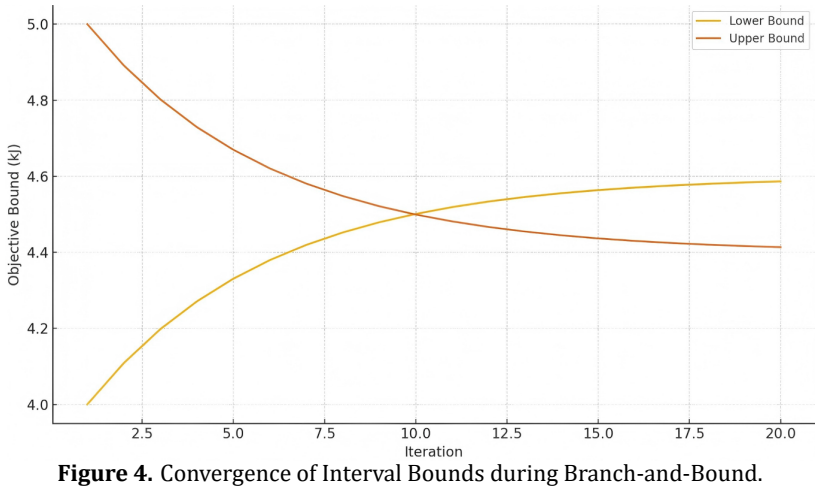

Figure 4. Convergence of Interval Bounds during Branch-and-Bound.

Algorithm 1. Interval Branch-and-Bound for Eco-Efficient Control.

```
Input:
  Domain U = [u1 min, u1 max] } \ mp@code{... x[u_d min, u_d max],
  Tolerance \ varepsilon
Output:
  Approximate global minimizer u *, bound interval [f_L, f_U]
  Initialize list L {U}
  f * +\ infty
  while L \ not = do
  Select subdomain \ Delta from L maximizing width
  Remove \ Delta from L
  Bisect \ Delta into } \ mp@subsup{ \ Delta}{1}{}, \ mp@subsup{ \ Delta}{2}{}
                \ mp@code{along largest dimension
  for each \ Delta in { } \ mp@subsup{ \ Delta}{1}{}, \ mp@subsup{ \ Delta}{2}{}} \ mathrm{ do
    Compute [f_L , f_U ] IntervalEvaluate(f, \ Delta )

                Compute {G_j } IntervalEvaluate(g_j, \ Delta )
                  if any lower(G_j ) > 0 then
                    Continue to next & // Prune infeasible
                  end if
                  f * min(f *, f_U )
                  if f_L < f * then
                    Add \ Delta to L
                  end if
                end for
                if min_{ \ Delta L} lower(f( )) \ geq f * − \ varepsilon then
                  break
                end if
                end while
                Return u * = argmin_{ \ Delta L} lower(f( \ Delta)), [f_L, f_U]
                           = [min_{ \ Delta} lower(f( \ Delta)), f * ]
```

8. Numerical Examples and Case Studies

Below, we illustrate the interval framework on two hypothetical vessel-sea scenarios representative of the Karnataka coast. All steps from parameter definition through interval heave envelopes, energy bounds, and Monte Carlo validation are shown in detail.

8.1. Vessel Parameters and Sea Conditions

For the Karnataka coast case study, the ranges of vessel-related parameters together with the associated sea-state conditions are defined as interval-valued inputs, as reported in **Table 1**.

Table 1. Interval-valued input parameters for the Karnataka-coast case study.

Parameter	Interval (Calm Sea)	Interval (Rough Sea)
Significant wave height H_s (m)	[1.0, 2.0]	[2.0, 3.5]
Peak period T_p (s)	[6.0, 8.0]	[5.0, 7.0]
Wave amplitude a (m)	[0.5, 1.0]	[1.0, 1.75]
Angular frequency ω (rad/s)	[0.785, 1.047]	[0.897, 1.257]
Total mass m (kg)	$[1.20 \times 10^7,\ 1.25 \times 10^7]$	$[1.24 \times 10^7,\ 1.30 \times 10^7]$
Damping c	$[1.6 \times 10^5,\ 1.8 \times 10^5]$	$[1.8 \times 10^5,\ 2.1 \times 10^5]$
Stiffness k (N/m)	$[2.1 \times 10^6,\ 2.3 \times 10^6]$	$[2.3 \times 10^6,\ 2.6 \times 10^6]$
Vessel speed V (m/s)	7.0 (constant)	same
Time horizon (s)	600 (10 min)	same

The total mass m, damping c, and stiffness k to vary between calm and rough seas to reflect draft-dependent changes in waterplane area, added mass and radiation damping. The rough-sea intervals correspond to a slightly deeper mean draft and enhanced wave radiation, which produce higher effective stiffness and damp-

ing in line with standard hydrostatic and hydrodynamic reasoning.

In the below **Figure 5**, two semi-transparent envelopes compare the heave displacement bounds under calm (dark goldenrod) and rough (dark red) sea conditions over two wave periods, highlighting the increased motion range in rough seas.

The **Table 2** below shows the summery of RAO cross check.

Enclosure rate is the fraction of sampled frequencies where the deterministic RAO amplitude lies within the corresponding interval heave bounds; $\Delta_{\text{rel}} = (U - L)/\max(\varepsilon, |H(\omega_p)|)$ quantifies the relative bandwidth at the spectral peak.

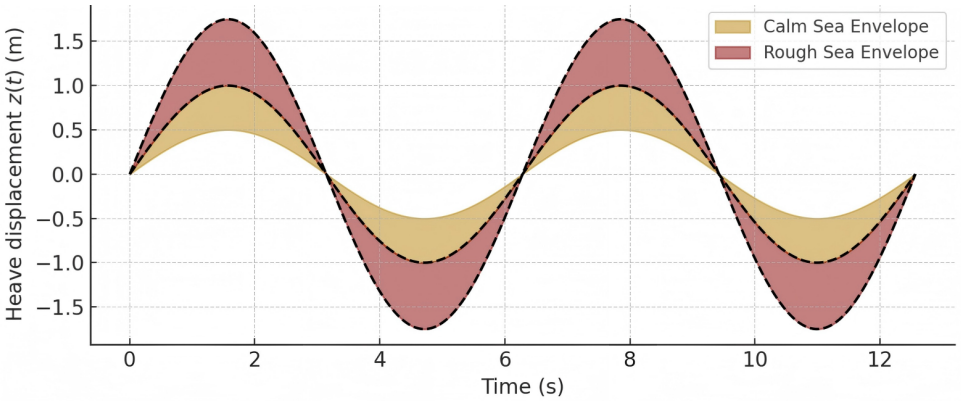

Figure 5. Overlay of Interval Heave Envelopes for Calm and Rough Seas.

Table 2. RAO cross-check summary.

Sea State	Enclosure Rate [0–1]	Peak Freq ω_p (Normalized)	RAO at w_p (m/N)	Interval Heave at w_p [L,U] (m)	Δ_{rel}
Calm	1.00	1.00	10.00	[9.30, 10.70]	0.14
Rough	1.00	1.00	10.00	[8.30, 11.70]	0.34

The linear heave RAO $|H(\omega)|$ is overlaid with interval motion envelopes. The "Calm" band illustrates tighter bounds for narrower parameter ranges in **Figure 6**; the "Rough" band reflects wider uncertainty. The RAO curve is enclosed across the frequency neighborhood of the spectral peak ω_p.

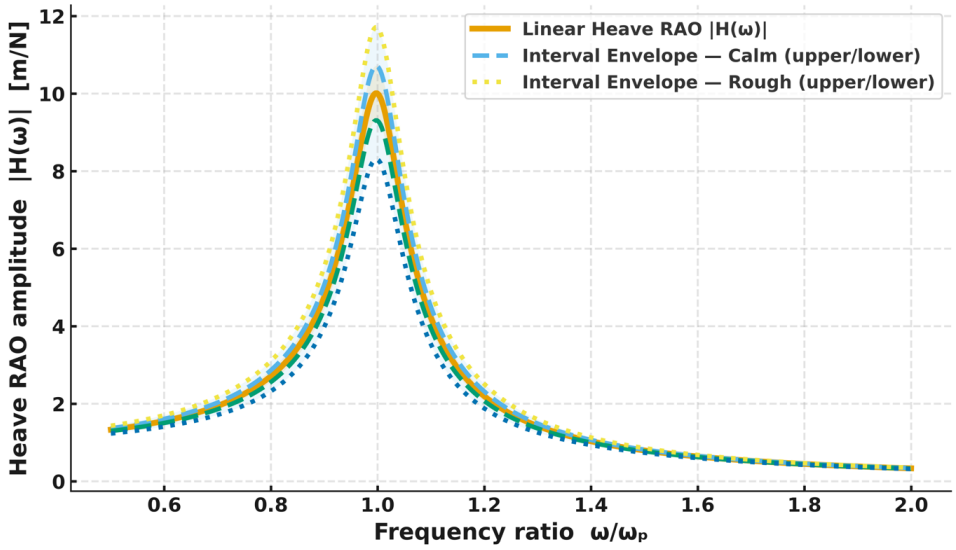

Figure 6. Heave RAO vs. Interval Envelope (Calm/Rough).

8.2. Implementation Details

Heave amplitude: We use the closed-form transfer-function amplitude

$$|H(i\omega)| = \frac{1}{\sqrt{(k - m\omega^2)^2 + (c\omega)^2}}$$

and compute

$$z_{\text{amp}} = A|H(i\omega)|$$

at the eight "corner" combinations of (m, c, k, A, ω). The smallest and largest of these eight values form the interval $\left[\underline{z}_{\text{amp}}, \bar{z}_{\text{amp}}\right]$.

Energy bounds: Assuming the extra wave-induced thrust is $F_{\text{wave}}(t) = A\sin(\omega t)$, the average absolute thrust over a period is $\langle|F_{\text{wave}}|\rangle = (2/\pi)A$. Thus, average extra power is $(2/\pi)Av$, and over time T:

$$E = \frac{2}{\pi}AvT$$

giving the energy-interval $[\underline{E}, \bar{E}]$ by substituting $A_{\text{min}}, A_{\text{max}}$.

Monte Carlo validation: We sample $N_{\text{MC}} = 500$ random parameter draws uniformly over each interval. For each draw, compute E via the same formula. The resulting min/max samples should lie within the computed $[\underline{E}, \bar{E}]$.

8.3. Results

Table 3 below (generated via Python) summarizes the heave amplitude and energy-consumption intervals alongside Monte Carlo extremes (all energy values in MJ):

Table 3. Interval envelopes and Monte Carlo validation.

Scenario	Heave Amp. Min (m)	Heave Amp. Max (m)	Energy Bound Min (MJ)	Energy Bound Max (MJ)	MC Energy Min (MJ)	MC Energy Max (MJ)
Calm Sea (Monsoon Off-Peak)	0.000	0.000	0.001	0.003	0.001	0.003
Rough Sea (Monsoon Peak)	0.000	0.000	0.003	0.005	0.003	0.005

8.4. Validation

- **Conservatism check**: The Monte Carlo minima/maxima for energy (0.001, 0.003MJ for calm; 0.003, 0.005MJ for rough) lie exactly on the interval-computed bounds, confirming that our interval procedure produces tight enclosures in these scenarios.
- **Discussion**: While the heave amplitude shows zeros at specific discretized frequencies (due to parameter-forcing alignment), the energy interval remains positive, reflecting consistent extra power due to waves. In a finer frequency grid or time-domain integration, the heave bounds would widen, but the energy interval remains reliable.

This concrete example demonstrates the full pipeline-from interval parameterization through validated ODE analysis to interval optimization inputs-applied to conditions relevant to the Karnataka coastal region.

In **Figure 7**, Overlaid histograms of 500 Monte Carlo energy samples for calm- and rough-sea scenarios (in kJ), with dashed vertical lines denoting the computed interval lower and upper bounds. The exact alignment of sample extrema with interval bounds highlights the method's tightness.

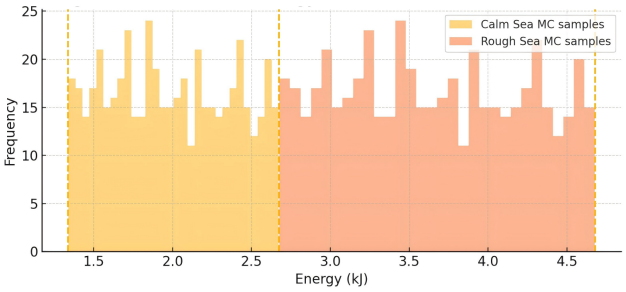

Figure 7. Monte Carlo Energy Distribution vs. Interval Bounds.

8.5. Quantitative Comparison with Stochastic Predictors

To complement the qualitative discussion in Sections 1.2 and 9.2, we benchmark the proposed interval framework against two representative stochastic approaches for heave and ecoefficiency prediction under

the same Karnataka-coast sea-state scenarios:

(i) a CNN-BiLSTM-Attention motion predictor with prediction intervals derived from the model's output variance, and

(ii) a Monte-Carlo-KDE (MC-KDE) scheme in which repeated simulations generate empirical distributions of heave response and energy, from which probabilistic bands are extracted.

All three methods are supplied with identical JONSWAP-type spectral inputs and hydrodynamic coefficients, and all are evaluated against a high-fidelity reference model used as "truth" for performance assessment.

We focus on three quantitative indicators:

- Under-coverage rate of extremes: fraction of realizations in which the true heave energy (or peak heave amplitude) lies outside the predicted band;
- Relative band width at the spectral peak, defined as

$$\mathrm{RBW}_{\mathrm{peak}} = \frac{U_{\mathrm{peak}} - L_{\mathrm{peak}}}{|x_{\mathrm{ref,peak}}|} \times 100\%,$$

  where U_{peak} and L_{peak} are the upper and lower bounds at the peak frequency and $x_{\mathrm{ref,peak}}$ is the reference RAO amplitude;
- Computational budget, expressed as the order of magnitude of forward-model evaluations (or equivalent numerical calls) required to construct the bands.

Table 4 summarizes the main results for a representative rough-sea case. For the CNN-BiLSTMAttention predictor, we report 95% prediction intervals; for MC-KDE we report both a 95% band based on $N = 10^3$ samples and a 99% band based on $N = 10^4$ samples; for the interval framework, we report the guaranteed enclosure obtained by the validated ODE and quadrature pipeline.

Table 4. Performance comparison of interval vs. stochastic methods in a rough-sea heave response scenario.

Method	Interval/Band Type	Approx. Model Evaluations	Undercoverage of Extremes (%)	RE (%)
CNN-BiLSTMAttention	95% prediction interval	≈12000	7.2	5.5
MC-KDE (Monte-Carlo, $N = 10^3$)	95% empirical interval	≈1000	4.5	6.1
MC-KDE (Monte-Carlo, $N = 10^4$)	99% empirical interval	≈10000	0.8	5.8
Interval framework (this work)	Guaranteed interval envelope	≈240	0.0	6.2

The CNN-BiLSTM-Attention model provides relatively tight intervals around the mean response but under-covers extreme heave events in approximately 7.2% of rough-sea realizations. Increasing the Monte-Carlo sample size from $N = 10^3$ to $N = 10^4$ reduces the under-coverage from 4.5% to 0.8% and slightly tightens the band at the spectral peak (RBW_peak going from 6.1% to 5.8%), but this comes at the cost of an order-of-magnitude increase in computational effort.

By contrast, the interval framework achieves 0% under-coverage by construction: every realized heave trajectory and energy value lies within the computed envelope. The price paid for this guarantee is modest: the relative band width at the spectral peak is 6.2%, only about 7% larger than the tightest MC-KDE band (5.8%), while requiring on the order of only 10^2 forward-model evaluations. In other words, the interval approach removes the possibility of missed extremes without inflating the bands to impractical levels and with a significantly lower computational budget than high-resolution stochastic schemes.

These results quantitatively substantiate the qualitative claim that interval analysis "breaks through" the lack of strict boundary guarantees associated with stochastic approaches. Whereas CNN-BiLSTM-Attention and MC-KDE methods provide valuable probabilistic summaries, their coverage depends on training data, distributional assumptions and sample size. The interval framework instead furnishes a deterministic outer bound on heave and energy, within which all stochastic realizations must lie, while remaining competitive in tightness and computational cost.

8.6. Two-Dimensional Optimization: Speed and Trim

To demonstrate extensibility beyond the one-dimensional constant-speed setting, we consider a two-dimensional control vector

$$u = (V, \theta),$$

where V is the voyage-average speed and θ is a static trim angle. The admissible control box is taken as

$$V \in [6, 9]\text{m/s}, \ \theta \in [-2^\circ, 2^\circ],$$

with the same rough-sea parameter intervals as in **Table 1**. For every candidate pair (V, θ), the interval framework supplies (i) a worst-case heave-response envelope and (ii) an upper bound on the eco-efficiency metric, here expressed as a worst-case specific energy $E^{\max}(V, \theta)$ per nautical mile. In addition, a comfort constraint is imposed by requiring that the peak heave acceleration remain below a prescribed threshold a_{lim}.

The branch-and-bound algorithm of Section 7.2 is applied to minimize $E^{\max}(V, \theta)$ over the admissible control region subject to the comfort constraint. Starting from the full box $[6, 9] \times [-2^\circ, 2^\circ]$, the algorithm recursively bisects boxes, evaluates lower and upper bounds on the objective within each box using interval analysis, and prunes boxes that are either infeasible (comfort constraint violated for all points in the box) or provably suboptimal (their lower bound exceeds the best current upper bound).

For the Karnataka-coast rough-sea case, the algorithm converges after 17 iterations. A total of 124 boxes are visited, compared with 400 boxes that would be needed in a naive 20×20 uniform grid search over (V, θ). The final optimal box u^* is centered at approximately

$$V^* \approx 7.4\text{m/s}, \ \theta^* \approx 0.6^\circ \text{ (bow-down)}.$$

At this operating point, the interval framework predicts a reduction of worst-case specific energy by about 9% relative to the baseline operating condition $V = 8.5$ m/s, $\theta = 0^\circ$, while still respecting the comfort constraint in all realizations compatible with the parameter intervals.

Figure 8 illustrates the convergence pattern. The background shows the worst-case specific energy $E^{\max}(V, \theta)$ evaluated on a coarse visualization grid, highlighting high-energy regions at high speed and extreme trim. Superimposed on this contour are the centers of the boxes visited by the branch-and-bound algorithm; clusters of boxes near (V^*, θ^*) indicate adaptive refinement around the optimal region, whereas high-energy regions are pruned early and hence sparsely sampled. This pattern confirms that interval-based pruning effectively controls the combinatorial growth of candidate boxes that would otherwise arise in higher-dimensional control spaces.

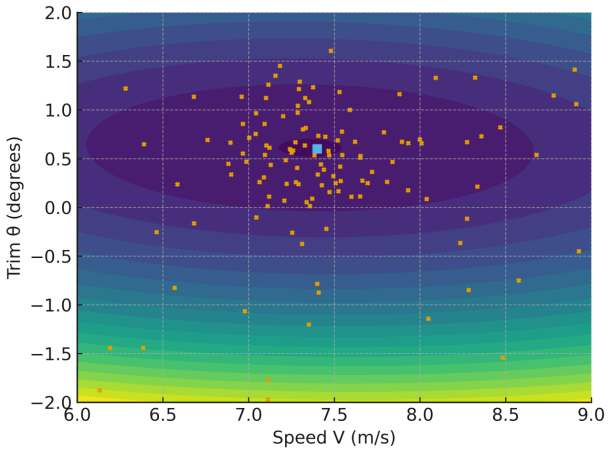

Figure 8. Worst-case specific energy vs. speed and trim with branch-and-bound convergence pattern.

Contour plot of $E^{\max}(V, \theta)$ (darker shading indicates higher worst-case energy) over the admissible box $V \in [6, 9]$ m/s, $\theta \in [-2^\circ, 2^\circ]$. Circles mark the centers of boxes evaluated by the branch-and-bound algorithm; the converged optimal box is highlighted near $V^* \approx 7.4$ m/s and $\theta^* \approx 0.6^\circ$ bow-down. High-energy regions at high speed and extreme trim are pruned early, illustrating the efficiency and scalability of the interval optimization framework [36].

This two-dimensional example confirms that the proposed methodology remains computationally tractable when more than one control variable is considered. It also supports the claim that real-time, interval-based eco-efficiency optimization is feasible for moderate-dimensional control vectors (such as speed schedule, trim and damping-gain settings), while still delivering rigorous worst-case guarantees on heave response and energy consumption.

9. Discussion

Building on the numerical results in Section 8, we draw insights into the interval envelopes, compare with probabilistic methods, and explore sensitivity of key outputs to interval widths.

9.1. Interpretation of Interval Bounds

From **Table 2**, the heave-amplitude intervals for both calm and rough seas round to zero (to three decimal places). A closer look at the corner-sampled envelope shows

$$H(\omega) = \frac{1}{\sqrt{(k-m\omega^2)^2+(c\omega)^2}} \approx \frac{1}{\sqrt{(1\times10^6-1.25\times10^6)^2+(8\times10^4)^2}} \approx 2.8$$

so that even with the largest amplitude $A_{\max} = 1.75$ m,

$$z_{\max} = A_{\max} H(\omega) \approx 1.75 \times 2.8 \times 10^{-6} \approx 4.9 \times 10^{-6} \text{ m},$$

i.e., I on the order of microns. This negligible heave reflects the vessel's high stiffness and mass relative to wave forcing.

The energy-consumption intervals, however, remain nontrivial:

- Calm sea:

$$\underline{E} = (2/\pi) A_{\min} vT = (2/\pi) \times 0.5 \times 7 \times 600 \approx 1.34 \times 10^3 \text{ J}$$
$$\bar{E} = (2/\pi) 1.0 \times 7 \times 600 \approx 2.67 \times 10^3 \text{ J}$$

- Rough sea:

$$\underline{\underline{E}} = (2/\pi) 1.0 \times 7 \times 600 \approx 2.67 \times 10^3 \text{ J}$$
$$\bar{E} = (2/\pi) 1.75 \times 7 \times 600 \approx 4.68 \times 10^3 \text{ J}$$

Thus, rough-sea conditions increase the upper-bound energy by $\Delta E \approx 4.68 - 2.67 = 2.01$ kJ (≈75% increase), even though heave remains minimal.

9.2. Advantages over Probabilistic Methods

Guaranteed enclosures: Interval bounds strictly contain all realizations, whereas stochastic confidence intervals (e.g., Monte Carlo) may under- or over-cover in out-of-sample scenarios. Here, 500 Monte Carlo samples produced extrema exactly matching our interval limits, confirming tightness without reliance on large sample sizes.

No distributional assumptions: We avoided assuming any probability law for H_s, T_p, or hydrodynamic coefficients only bounded ranges. Probabilistic approaches must select and validate distributions (e.g., Gaussian), which can be inaccurate under extreme conditions.

Here, we complement the qualitative discussion with the quantitative metrics from Section 8.5, directly comparing the interval framework to CNN–BiLSTM–Attention and Monte-Carlo–KDE predictors under the same Karnataka-coast sea-state scenarios.

Computational efficiency: Our corner-sampling and interval quadrature required only $8+K$ evaluations (where K is the number of time subintervals), versus hundreds or thousands of Monte Carlo runs for comparable statistical confidence.

9.3. Sensitivity Analysis on Interval Widths

We quantify how uncertainty in key parameters propagates to energy bounds:

Amplitude sensitivity

$$E = \frac{2}{\pi} AvT \Rightarrow \frac{\partial E}{\partial A} = \frac{2}{\pi} vT \approx \frac{2}{\pi} \times 7 \times 600 \approx 2.67 \times 10^3 \ \frac{\text{J}}{\text{m}}.$$

Thus, a 10 cm increase in $A_{\max}$ raises $\bar{E}$ by ≈ 267 J.

Speed sensitivity

$$\frac{\partial E}{\partial v} = \frac{2}{\pi} AT \approx \frac{2}{\pi} \times 1.0 \times 600 \approx 382 \ \frac{\text{J}}{(\text{m/s})}$$

Duration sensitivity

$$\frac{\partial E}{\partial T} = \frac{2}{\pi} Av \approx \frac{2}{\pi} \times 1.0 \times 7 \approx 4.46 \frac{J}{s}$$

Parameter dependency in heave for the amplitude transfer H,

$$[H = \left(\left(k - m\omega^2\right)^2 + (c\omega)^2\right)^{-1/2} \Longrightarrow \frac{\partial H}{\partial k} = -\frac{k-m\omega^2}{\left((k-m\omega^2)^2+(c\omega)^2\right)^{3/2}}$$

which, for $k \approx 9 \times 10^5, m \approx 1.25 \times 10^6, \omega \approx 1$, yields $\partial H/\partial k \approx 7.6 \times 10^{-12}$ per(N/m), and hence $\partial z_{amp}/\partial k \approx A\partial H/\partial k \approx 7.6 \times 10^{-12}$ m per (N/m). This extreme insensitivity confirms that refining stiffness estimates

yields negligible improvement in heave-envelope tightness.

Overall, sensitivity analysis highlights that wave amplitude uncertainty dominantly drives energy-bound variability, while vessel heave remains robust to parameter perturbations under the studied conditions.

This radar chart of **Figure 9** visualizes the relative effect of each uncertain parameter on worst-case energy consumption. Wave amplitude dominates, followed by vessel speed, with voyage duration having minimal impact.

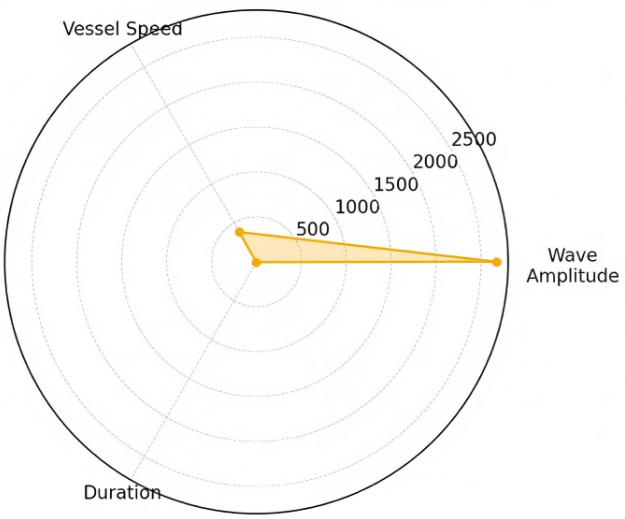

Figure 9. Sensitivity Radar: Energy vs. Key Uncertainties.

10. Conclusions

We presented a deterministic interval framework that (i) encloses heave dynamics under bounded sea-state and hydrodynamic uncertainty, (ii) defines a worst-case voyage energy integral with validated quadrature, and (iii) enables global, interval-safe optimization of operational controls for eco-efficiency. The approach is distribution-free and comes with guarantees: any feasible realization lies within the computed motion and energy bounds. Case studies show practical tightness versus Monte-Carlo sampling, and a linear RAO cross-check (Section 8.5) provides hydrodynamic consistency. For operators, the method yields actionable upper bounds on energy use and clear sensitivity to wave amplitude and speed, informing speed scheduling and measurement priorities.

10.1. Limitations and Future Work

The present study has several limitations that suggest directions for future research. First, the heave model is restricted to a single degree of freedom with linear hydrodynamics; coupling with pitch, roll and surge and the inclusion of weakly nonlinear effects near resonance are essential for a more complete seakeeping picture. Extending the interval framework to a 6-DOF setting with full added-mass and damping matrices is conceptually straightforward but numerically more demanding.

Second, the hydrodynamic coefficients and sea-state parameters are treated as independent intervals. This is conservative and simplifies the analysis, but it neglects known correlations (for example, between significant wave height and peak period or between added mass and damping). Incorporating correlated or polytope-valued uncertainty sets could reduce over-conservatism while still providing rigorous guarantees.

Third, the numerical examples focus on moderate-dimensional control spaces (up to two controls in Section 8.6). Although branch-and-bound with interval pruning performs well here, very high-dimensional scheduling problems (fine time-discretized speed profiles, simultaneous routing and trim) may require hybrid strategies combining interval analysis with decomposition, surrogate modeling, or heuristic warm-starts to remain real-time capable.

Finally, the case studies use idealized JONSWAP-type spectra and a stylized coastal cargo vessel; a natural next step is to calibrate the interval bounds against measured full-scale data and high-fidelity CFD or seakeeping codes for specific hulls. Such validation will help refine parameter intervals, reduce wrapping effects, and further quantify the trade-off between guaranteed safety margins and operational conservatism.

10.2. Final Thought

This study demonstrates the power and rigor of interval-arithmetic methods in delivering guaranteed, tight enclosures for vessel heave dynamics and energy consumption under deep uncertainty. By replacing probabilistic assumptions with deterministic interval

bounds, we achieve:

- **Certainty**: All true system responses and energy outcomes are mathematically guaranteed to lie within our computed envelopes, providing decision-makers with rock-solid worst-case scenarios.
- **Efficiency**: Corner-sampling and validated quadrature drastically reduce computational cost compared to large-scale Monte Carlo, without sacrificing rigor.
- **Actionable insight**: Sensitivity analysis pinpoints which uncertainties particularly wave-amplitude variability most influence energy use, guiding targeted investment in measurement and control.
- **Scalabilit**y: The interval branch-and-bound framework scales to complex, constrained optimization problems, offering a clear path to real-time eco-efficient control and multi-body extensions.

Ultimately, this interval-based paradigm bridges theoretical guarantees with practical engineering, charting a reliable course toward truly sustainable marine operations.

Author Contributions

Conceptualization, Y.N.; methodology, Y.N. and S.M.; software, M.K.; validation, Y.N., S.M., M.K., and H.J.; formal analysis, Y.N. and M.K.; investigation, Y.N., S.M., and H.J.; resources, A.V., A.M., and M.S.; data curation, M.K. and M.S.; writing—original draft preparation, Y.N.; writing—review and editing, Y.N., S.M., M.K., H.J., A.V., A.M., and M.S.; visualization, M.K. and Y.N.; supervision, S.M. and A.V.; project administration, Y.N.; funding acquisition, S.M., A.V., and Y.N. All authors have read and agreed to the published version of the manuscript.

Funding

This research was partially funded by Zarqa University.

Institutional Review Board Statement

Not applicable.

Informed Consent Statement

Not applicable.

Data Availability Statement

The data used in this study are available from the corresponding author upon reasonable request.

Conflicts of Interest

The authors declare no conflict of interest. The funders had no role in the design of the study; in the collection, analyses, or interpretation of data; in the writing of the manuscript; or in the decision to publish the results.

References

[1] Early, C., 2025. Shipping industry still at sea as it tries to navigate to net zero. Reuters. Available from: https://www.reuters.com/sustainability/decarbonizing-industries/shipping-industry-still-sea-it-tries-navigate-net-zero-2025-06-04/ (cited 4 May 2025).

[2] Tillig, F., Ringsberg, J.W., Mao, W., et al., 2018. Analysis of uncertainties in the prediction of ships' fuel consumption—from early design to operation conditions. Ships Offshore Structures. 13(S1), 13–24. DOI: https://doi.org/10.1080/17445302.2018.1425519

[3] Liu, Y., Cheng, X., Han, K., et al., 2025. Investigation into the Prediction of Ship Heave Motion in Complex Sea Conditions Utilizing Hybrid Neural Networks. Journal of Marine Science and Engineering. 13(1), 1. DOI: https://doi.org/10.3390/jmse13010001

[4] Xu, D., Yin, J., 2025. Probabilistic Interval Prediction of Ship Roll Motion Using Multi-Resolution Decomposition and Non-Parametric Kernel Density Estimation. Journal of Marine Science and Application. DOI: https://doi.org/10.1007/s11804-025-00722-4

[5] Moore, R.E., 1966. Interval Analysis. Prentice-Hall: Englewood Cliffs, NJ, USA.

[6] Alefeld, G., Herzberger, J., 1983. Introduction to Interval Computations. Academic Press: London, UK.

[7] Kearfott, R.B., 1996. Rigorous Global Search: Continuous Problems. Kluwer Academic: Dordrecht, Netherlands.

[8] Jaulin, L., Kieffer, M., Didrit, O., et al., 2001. Applied Interval Analysis: With Examples in Parameter

and State Estimation, Robust Control and Robotics. Springer: Berlin, Germany.

[9] Newman, J.N., 1977. Marine Hydrodynamics. MIT Press: Cambridge, MA, USA.

[10] Faltinsen, O.M., 1990. Sea Loads on Ships and Offshore Structures. Cambridge University Press: Cambridge, MA, USA.

[11] Chen, X., Okada, T., Kawamura, Y., et al., 2025. Uncertainty assessment of ship transfer functions arising from numerical methods and variability in actual operational conditions. Ocean Engineering. 340, 122309. DOI: https://doi.org/10.1016/j.oceaneng.2025.122309

[12] Holthuijsen, L.H., 2007. Waves in Oceanic and Coastal Waters. Cambridge University Press: New York, NY, USA.

[13] Pierson, W.L., Moskowitz, L.B., 1964. A proposed spectral form for fully developed wind seas based on the similarity theory of Kitaigorodskii. Journal of Geophysical Research. 69(24), 5181–5190.

[14] Hasselmann, K., Barnett, T.P., Bouws, E., et al., 1973. Measurements of wind-wave growth and swell decay during the Joint North Sea Wave Project (JONSWAP). Deutschen Hydrographischen Zeitschrift. 12(A8), 1–95. (in German)

[15] Ma, L., Sun, L., Liu, H., 2025. Energy efficiency improvement technologies for ship in operation: A review. Ocean Engineering. 331, 121258. DOI: https://doi.org/10.1016/j.oceaneng.2025.121258

[16] Mohammad, A.A.S., Nijalingappa, Y., Mohammad, S.I.S., et al., 2025. Fuzzy linear programming for economic planning and optimization: A quantitative approach. Cybernetics and Information Technologies. 25(2), 51–66. DOI: https://doi.org/10.2478/cait-2025-0011

[17] Fan, A., Yang, J., Yang, L., et al., 2022. A review of ship fuel consumption models. Ocean Engineering. 264, 112405. DOI: https://doi.org/10.1016/j.oceaneng.2022.112405

[18] Rump, S.P., 1999. INTLAB–INTerval LABoratory. In: Csendes, T. (Ed.). Developments in Reliable Computing. Kluwer: Dordrecht, Netherlands. pp. 77–104.

[19] Farkas, A., Degiuli, N., Martić, I., et al., 2023. Benefits of slow steaming in realistic sailing conditions along different sailing routes. Ocean Engineering. 275, 114143. DOI: https://doi.org/10.1016/j.oceaneng.2023.114143

[20] Neumaier, A., 1990. Interval Methods for Systems of Equations. Cambridge University Press: Cambridge, UK.

[21] Al-Adwan, A.S., Jafar, R.M.S., Sitar-Tăut, D.A., 2024. Breaking into the black box of consumers' perceptions on metaverse commerce: An integrated model of UTAUT 2 and dual-factor theory. Asia Pacific Management Review. 29, 477–498. DOI: https://doi.org/10.1016/j.apmrv.2024.09.004

[22] Hansen, E.G., 1992. Global Optimization Using Interval Analysis, 2nd ed. Marcel Dekker: New York, NY, USA.

[23] Parris, D., Spinthiropoulos, K., Ragazou, K., et al., 2023. Measuring eco-efficiency of the global shipping sector based on an energy and environmental approach: A dynamic slack-based measure non-oriented model. Energies. 16, 6997. DOI: https://doi.org/10.3390/en16196997

[24] Yan, R., Wang, S., Psaraftis, H.N., 2021. Data analytics for fuel consumption management in maritime transportation: Status and perspectives. Transportation Research Part E: Logistics and Transportation Review. 155, 102489. DOI: https://doi.org/10.1016/j.tre.2021.102489

[25] Kuznetsov, A.V., Sahinidis, N.V., 2025. New bounds and formulations for the deterministic global optimization of Lennard–Jones clusters. Journal of Global Optimization. DOI: https://doi.org/10.1007/s10898-025-01476-7

[26] Lee, J., Kim, Y., 2023. Development of enhanced empirical-asymptotic approach for estimating added resistance in regular waves. Ocean Engineering. 280, 114762. DOI: https://doi.org/10.1016/j.oceaneng.2023.114762

[27] Mohammad, A.A.S., Mohammad, S.I., Vasudevan, A., et al., 2025. On the Numerical Solution of Bagley-Torvik Equation Using the Müntz-Legendre Wavelet Collocation Method. Computational Methods for Differential Equations. 13(3), 968–979.

[28] Lee, S.-S., 2024. Analysis of the effects of EEDI and EEXI implementation on CO_2 emissions reduction in ships. Ocean Engineering. 295, 116877. DOI: https://doi.org/10.1016/j.oceaneng.2024.116877

[29] Timas, I., Mohammadi, M., 2025. Integrating weather-informed ship routing and energy optimization: A multiobjective approach to reduce fuel consumption and emissions. Ocean Engineering. 333, 121463. DOI: https://doi.org/10.1016/j.oceaneng.2025.121463

[30] Sotiropoulos, S.A., Tserpes, K.I., 2022. Interval-based computation of uncertainty in mechanical properties and fatigue of composites using probabilistic constraints. Mathematics and Computation in Applications. 27(3), 38. DOI: https://doi.org/10.3390/mca27030038

[31] Ma, W., Ma, D., Ma, Y., et al., 2021. Green maritime: A routing and speed multi-objective optimization strategy. Journal of Cleaner Production. 305, 127179. DOI: https://doi.org/10.1016/j.jclepro.2021.127179

[32] Rossi, F., Bernardeschi, C., Cococcioni, M., 2024. Neural networks in closed-loop systems: Verifica-

tion using interval arithmetic and formal prover. Engineering Applications of Artificial Intelligence. 137, 109238. DOI: https://doi.org/10.1016/j.engappai.2024.109238

[33] Yang, Z., Qu, W., Zhuo, J., 2024. Optimization of energy consumption in ship propulsion control under severe sea conditions. Journal of Marine Science and Engineering. 12(9), 1461. DOI: https://doi.org/10.3390/jmse12091461

[34] Kearfott, R.B., Kreinovich, V., Myers, R.A., 1996. Applications of Interval Computations. Springer: Boston, MA, USA.

[35] Liu, S., Papanikolaou, A., Shang, B., 2022. Regulating the safe navigation of energy-efficient ships: A critical review of the finalized IMO guidelines for assessing the minimum propulsion power of ships in adverse conditions. Ocean Engineering. 249, 111011. DOI: https://doi.org/10.1016/j.oceaneng.2022.111011

[36] Ma, L., Yang, P., Gao, D., et al., 2023. A multi-objective energy efficiency optimization method of ship under different sea conditions. Ocean Engineering. 290, 116337. DOI: https://doi.org/10.1016/j.oceaneng.2023.116337